ADVANCES IN ATMOSPHERIC SCIENCES, VOL. 37, JUNE 2020, 597–607

• Original Paper •

Deriving Temporal and Vertical Distributions of Methane in Xianghe Using Ground-based Fourier Transform Infrared and Gas-analyzer Measurements

Denghui JI[1,3], Minqiang ZHOU[*2], Pucai WANG[1,3], Yang YANG[1,2,3], Ting WANG[1,3], Xiaoyu SUN[1,3], Christian HERMANS[2], Bo YAO[4], and Gengchen WANG[1]

[1]*Key Laboratory of Middle Atmosphere and Global Environment Observation*, *Institute of Atmospheric Physics*, *Chinese Academy of Sciences*, *Beijing* 100029, *China*

[2]*Royal Belgian Institute for Space Aeronomy*, *Brussels* 1180, *Belgium*

[3]*University of Chinese Academy of Sciences*, *Beijing* 100049, *China*

[4]*Meteorological Observation Center*, *China Meteorological Administration*, *Beijing* 100081, *China*

(Received 28 October 2019; revised 26 February 2020; accepted 3 March 2020)

ABSTRACT

Methane (CH_4) is one of the most important greenhouse gases in the atmosphere, making it worthwhile to study its temporal and vertical distributions in source areas, e.g., North China. For this purpose, a ground-based high-resolution Fourier transform infrared spectrometer (FTIR), the Bruker IFS 125HR, along with an in-situ instrument, the Picarro G2301, were deployed in Xianghe County (39.8°N,117.0°E), Hebei Province, China. Data have been recorded since June 2018. For the FTIR measurements, we used two observation modes to retrieve the mole fraction of CH_4: the Total Carbon Column Observing Network (TCCON) method (retrieval algorithm: GGG2014), and the Network for the Detection of Atmospheric Composition Change (NDACC) method (retrieval algorithm: SFIT4). Combining FTIR with in-situ measurements, we found the temporal and vertical distributions of atmospheric CH_4 within three vertical layers (near the ground, in the troposphere, and in the stratosphere), and throughout the whole atmosphere. Regarding the diurnal variation of CH_4 near the ground, the concentration at night was higher than during the daytime. Regarding the seasonal variation, CH_4 was low in spring and high in summer, for all three vertical layers. In addition, there was a peak of CH_4 in winter near the ground, both in the troposphere and the whole atmosphere. We found that variation of CH_4 in the tropospheric column was close to that of the in-situ measurements near the ground. Furthermore, the variations of CH_4 in the stratospheric column could be influenced by vertical motions, since it was higher in summer and lower in winter.

Key words: methane, Fourier transform infrared spectrometer (FTIR), Picarro, retrieval method, source emissions

Citation: Ji, D. H., and Coauthors, 2020: Deriving temporal and vertical distributions of methane in Xianghe using ground-based Fourier transform infrared and gas-analyzer measurements.. *Adv. Atmos. Sci.*, **37**(6), 597–607, https://doi.org/10.1007/s00376-020-9233-4.

Article Highlights:

- A new FTIR measurement site began operating in Xianghe in June 2018, using both the TCCON and NDACC methods.
- Regarding the seasonal variation of CH_4, the FTIR total column amounts were highest in August (about 1.95 ppm) and December (about 1.92 ppm).
- Regarding the diurnal variation of CH_4 near the ground, the concentration at night was higher than that during the daytime.
- FTIR measurements suggest that variation of CH_4 in the stratospheric column is influenced by vertical motions.

1. Introduction

Since the beginning of the Industrial Revolution (1750), human activities have had a huge impact on the concentration of trace gases in the atmosphere. Anthropogenic greenhouse gas emissions from industry and agriculture, the burning of fossil fuels, destruction of surface vegetation, and changes in land type have led to a surge in atmospheric carbon dioxide (CO_2), from 280 ppm before the Industrial

* Corresponding author: Minqiang ZHOU
Email: minqiang.zhou@aeronomie.be

Revolution to 407.96 ppm in 2018. A rapid growth rate remains apparent. Methane (CH_4) rose from 0.722 ppm before the Industrial Revolution to 1.855 ppm in 2018. The increase of greenhouse gases could increase the greenhouse effect, and any increase in the average temperature of the Earth will have a huge impact on its ecosystems. The Intergovernmental Panel on Climate Change (IPCC) reported that a 2°C increase in the Earth's average temperature will be hazardous (IPCC, 2014), and Mann et al. (2014) predicted that this threshold would be exceeded by 2036. Therefore, monitoring and controlling greenhouse gas emissions is extremely important.

CH_4 is one of the most important carbon-containing compounds in the atmosphere. The global warming potential (GWP) of CH_4 is 28 times greater than that of CO_2 (IPCC, 2014). In addition, it is a chemically active gas, which can be oxidized in the atmosphere to form hydroxides and carbon oxyhydroxides. Stratospheric CH_4 can also react with chlorine atoms generated by photolysis of chlorofluorocarbons, inhibiting the destruction of stratospheric ozone by chlorine atoms (Duncanand Truong, 1955). The lifetime of CH_4 in the atmosphere is approximately nine years (Kirschke et al., 2013). Considering the GWP and lifetime of CH_4, it is important to study the sources and sinks of CH_4 to learn how to control it.

Generally, sources of CH_4 can be divided into two types: natural and anthropogenic. Natural sources include wetlands, vegetation, and oceans (Fung et al., 1991). Anthropogenic sources include energy activities (involving coal mining and oil and gas systems), agricultural activities (involving ruminants, rice field discharge, and open burning of straw), waste treatment (of solid waste, industrial waste, and domestic sewage) and constructed wetlands (Janssens-Maenhout et al., 2019). The destructive reaction with the hydroxyl radical (OH) is the biggest sink of CH_4 in the atmosphere, especially in the troposphere (Heilig, 1994).

Systematic observation of CH_4 began in the 1880s via the Global Atmospheric Watch (GAW) of the World Meteorological Organization (WMO). Currently, the ground-based high-resolution Fourier transform infrared (FTIR) solar absorption spectrometer plays an important role in remote sensing of trace gases. There are two CH_4 observation networks in the world: one is the Total Carbon Column Observing Network (TCCON) (Wunch et al., 2011), and the other is the Network for the Detection of Atmospheric Composition Change-Infrared Working Group(NDACC-IRWG) (De Mazière et al., 2018). Both networks exist in Europe, North America, and Japan, and there is currently only one potential additional TCCON site (in Hefei), and no NDACC site in China. In this study, the temporal and vertical distributions of CH_4were measured by both the FTIR in-situ techniques at a new site in Xianghe, China.

2. Observation site

Xianghe (39.8°N, 117.0°E) is located in Hebei Province in China, approximately 30 m above sea level and 50 km from Beijing. Figure 1a shows the location of this site, along with EDGAR v4.3.2 (Emission Database for Global Atmosphere Research) emission data (Janssens-Maenhout et al., 2019, Crippa et al., 2018). It is clear that Xianghe is in an area with high CH_4 emissions, of about 450–1200 tm^{-2} yr^{-1}. Thus, Xianghe is an appropriate site to gather information about CH_4 sources. It also has a continental monsoon climate, characterized by low precipitation amounts, higher winds and evaporation amounts in the spring, high temperatures, humidity, and intense rain in the summer, relatively less rainfall and calmer weather in the autumn, and cold and dry winds from the north in winter.

We began measuring CH_4 in June 2018. The sources of CH_4 are relatively variable and location-dependent. In most parts of the world, natural emissions are the main sources, such as wetlands, termites, oceans, and hydrates (Kaplan et al., 2006; IPCC, 2014; Zhang and Liao, 2015). However, more recently, anthropogenic emissions have come to play an important role (Kirschke et al., 2013). Fugitive emissions from solid fuels, rice cultivation and enteric fermentation are very important in China (Fig. 1b).

3. Instrumentation and methods

3.1. *Picarro G2301*

The Picarro G2301 gas mole fraction analyzer provides simultaneous and precise measurements of CO_2, CH_4, and H_2O, with a sensitivity of 1 ppb and negligible drift. This instrument is widely used in atmospheric science and air quality applications for quantification of emissions. The G2301 uses WS-CRDS (wavelength-scanning cavity ring-down spectroscopy) to measure the laser ring-down time difference over a path length of up to 20 km with high accuracy (Fang et al., 2012). It meets the WMO and ICOS (Integrated Carbon Observation System) performance requirements for CO_2 and CH_4 atmospheric monitoring (Laurent, 2015). The G2301 was fully operational, almost without interruption, during the study period. We use 5-min-averaged CH_4 data at the surface (90 mMSL) to ensure high accuracy (< 0.7 ppb).

3.2. *FTIR spectrometer*

We used the Bruker IFS 125HR FTIR to observe CH_4 in Xianghe, which is the highest-precision instrument among ground-based remote sensing instruments (± 0.9 ppb; Esler et al., 2000). The maximum optical path difference of the FTIR in Xianghe was 180 cm, with a spectral resolution of 0.0035 cm^{-1}. To obtain more observations of trace gases, we used two observation modes: TCCON and NDACC-IRWG. NDACC-IRWG adopts a CaF_2 beam splitter and an InSb detector with a spectral range of 1800–5400 cm^{-1}, while TCCON uses CaF_2 and InGaAs with a spectral range of 3900–12000 cm^{-1}. The FTIR works during the day [between 0900 and 1600 local time (LT)]. For each day, there are approximately 40 spectra measured in TCCON observation mode and 5 measured in NDACC observation mode, and these are used to retrieve CH_4. Figure 2 shows the typical spectra measured by the two modes. The

TCCON and NDACC retrieval strategies, i.e., retrieval windows and interfering species, are shown in Table 1. A specific filter is applied for the InSb spectrato increase the signal-to-noise ratio.

3.2.1. *Retrieval method*

The optimal estimation method (Rodgers, 2000) was applied to retrieve gas mole fractions from the FTIR solar

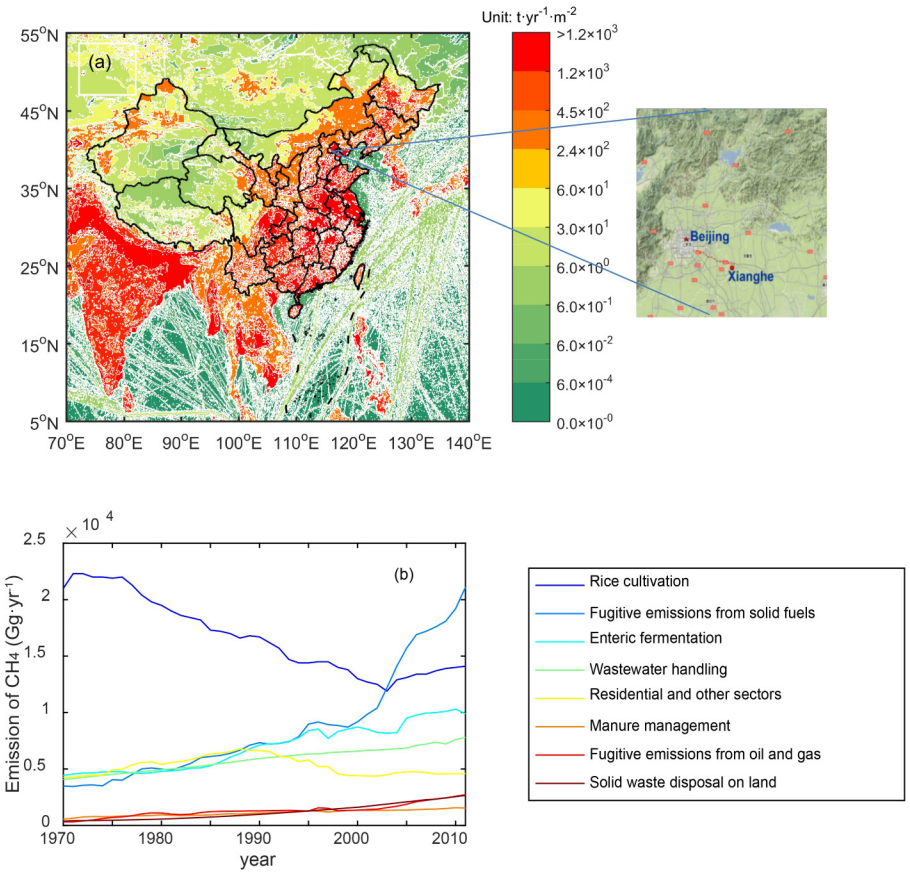

Fig. 1. (a) EDGAR v4.3.2 CH_4 anthropogenic emissions in 2012 in China. (b) Annual total Chinese CH_4 emissions contributed by eightsectors in 1970–2012.

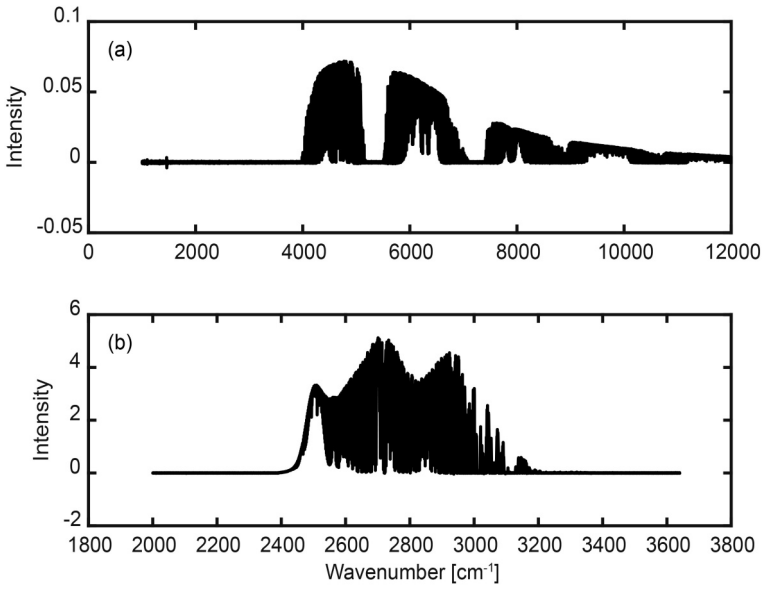

Fig. 2. Spectrum observed by FTIR with (a) InGaAs detector and (b) InSb detector.

Table 1. TCCON and NDACC CH_4 retrieval strategies in Xianghe.

Observation modes	TCCON	NDACC
Algorithm	GGG2014	SFIT4
Retrieval windows (cm^{-1})	5872.0–5988.0	2611.6–2613.35
	5996.45–6007.55	2613.7–2615.4
	6007.0–6145.0	2835.55–2835.8
		2903.82–2903.925
		2941.51–2942.22
Interfering species	CO_2, H_2O, N_2O	H_2O, HDO,CO_2, NO_2
A priori profile	TCCON tool (daily)	WACCM v4
Products	Total column	Profile

spectra. Several software retrieval algorithms are applied for different purposes, such as GGG2014, SFIT, and PROFFIT (Toon et al., 1992; Notholt et al., 1993; Hase et al., 2004).

According to the optimal estimation method, atmospheric radiation transfer can be described by a simple mathematical model, as follows:

$$\boldsymbol{Y} = \boldsymbol{F}(\boldsymbol{X}, \boldsymbol{b}) + \boldsymbol{\varepsilon}\,, \tag{1}$$

where $\boldsymbol{Y}$ is the radiation spectrum, $\boldsymbol{X}$ is the set of unknown atmospheric and surface state quantities, as well as the solar and instrumental parameters that affect the radiation spectrum, $\boldsymbol{b}$ is the set of known atmospheric and surface state parameters, $\boldsymbol{F}$ is the forward-transfer radiation model function, and $\boldsymbol{\varepsilon}$ is the error of observation. The inversion process involves taking the observed spectrum ($\boldsymbol{Y}$) and finding the unknown atmospheric and surface state parameters ($\boldsymbol{X}$).

To carry out the inversion process, a cost function is defined as:

$$J(\boldsymbol{X}) = (\boldsymbol{Y} - \boldsymbol{F}(\boldsymbol{X}, \boldsymbol{b}))^{\mathrm{T}} \boldsymbol{S}_{\epsilon}^{-1} (\boldsymbol{Y} - \boldsymbol{F}(\boldsymbol{X}, \boldsymbol{b})) + (\boldsymbol{X} - \boldsymbol{X}_{\mathrm{a}})^{\mathrm{T}} \boldsymbol{S}_{\mathrm{a}}^{-1} (\boldsymbol{X} - \boldsymbol{X}_{\mathrm{a}})\,, \tag{2}$$

where the first term on the right-hand side represents the difference between the measured and simulated spectra for a given atmospheric state of $\boldsymbol{X}$ and b, $\boldsymbol{S}_{\epsilon}$ is the noise covariance matrix, the second term on the right-hand side is the regularization term, constraining the atmospheric solution state $\boldsymbol{X}$ to the a priori state $\boldsymbol{X}_{\mathrm{a}}$, and $\boldsymbol{S}_{\mathrm{a}}$ is the a priori covariance matrix. Since most physical processes in the atmosphere are nonlinear, the cost function, Eq. (2), is minimized iteratively by the Levenburg-Marquardt (LM) Gauss–Newton method. Convergence gives the retrieved state vector, $\hat{\boldsymbol{x}}$, as follows:

$$\hat{\boldsymbol{x}} = \boldsymbol{x}_{\mathrm{a}} + \boldsymbol{A}(\boldsymbol{x}_t - \boldsymbol{x}_{\mathrm{a}}) + \boldsymbol{\varepsilon}\,, \tag{3}$$

where $\boldsymbol{x}_{\mathrm{a}}$ is the a priori state matrix, $\boldsymbol{x}_t$ is the true state vector, and $\boldsymbol{A}$ is the average kernel (AVK) function matrix, representing the sensitivity of the inversion parameters to the true state of the atmosphere, given by:

$$\boldsymbol{A} = \boldsymbol{G}\boldsymbol{K} = [(1+\gamma)\boldsymbol{S}_{\mathrm{a}}^{-1} + \boldsymbol{K}^{\mathrm{T}}\boldsymbol{S}_{\epsilon}^{-1}\boldsymbol{K}]^{-1}\boldsymbol{K}^{\mathrm{T}}\boldsymbol{S}_{\epsilon}^{-1}\boldsymbol{K}\,. \tag{4}$$

In Eq. (4), $\boldsymbol{G}$ is called the contribution function matrix, which indicates the contribution of observed values to inversion values, $\boldsymbol{K}$ is a weight function matrix that expresses the sensitivity of simulated values to input parameters, such as the instrument line functions, and γ is the coefficient in the LM method.

3.2.2. *GGG2014 and SFIT4 retrievals*

The GGG2014 algorithm was applied to retrieve the column-averaged dry-air mole fraction of CH_4 (X_{CH_4}) from InGaAs spectra. It also performs profile scaling. Specifically, X_{CH_4} is obtained from the ratio between the total column of CH_4 (VC_{CH_4}) and O_2 (VC_{O_2}), using the following equation:

$$X_{CH_4} = 0.2095 \frac{VC_{CH_4}}{VC_{O_2}}\,, \tag{5}$$

where 0.2095 is the volume mixing ratio of O_2 in dry air (Wunch et al., 2011).

Since there is no O_2 signal available in the mid-infrared spectrum, and the N_2 signal is very weak (Zhou et al., 2018), the SFIT4 algorithm calculates the X_{CH_4} from the dry-air column as follows:

$$X_{CH_4} = \frac{TC_{CH_4}}{\frac{P_{\mathrm{s}}}{g m_{\mathrm{air\_dry}}} - TC_{H_2O}\frac{m_{H_2O}}{m_{\mathrm{air\_dry}}}}\,, \tag{6}$$

where TC_{H_2O} is the total column of H_2O, P_{s} is the surface pressure, g is the column-averaged gravitational acceleration, and m_{H_2O} and $m_{\mathrm{air\_dry}}$ are the molecular masses of H_2O and dry air, respectively.

Note that the a priori information is different between GGG2014 and SFIT4. For the meteorological variables of temperature, pressure, and water vapor, both algorithms use NCEP six-hourly reanalysis data. However, the a priori profiles of CH_4 are obtained by different methods. For GGG2014, the daily profiles are generated by a stand-alone tool based on in-situ and aircraft measurements (Toon and Wunch, 2015). For SFIT4, the profiles are derived from the Whole Atmosphere Community Climate Model (WACCM), version 4 (Zhou et al., 2019).

Figure 3 shows information about the AVK in GGG2014 and SFIT4 for different solar zenith angles (SZAs). The AVK represents the sensitivity of the inversion to the true state of the atmosphere (see section 3.2.1). Ideally, the AVK is an identity matrix, indicating that the

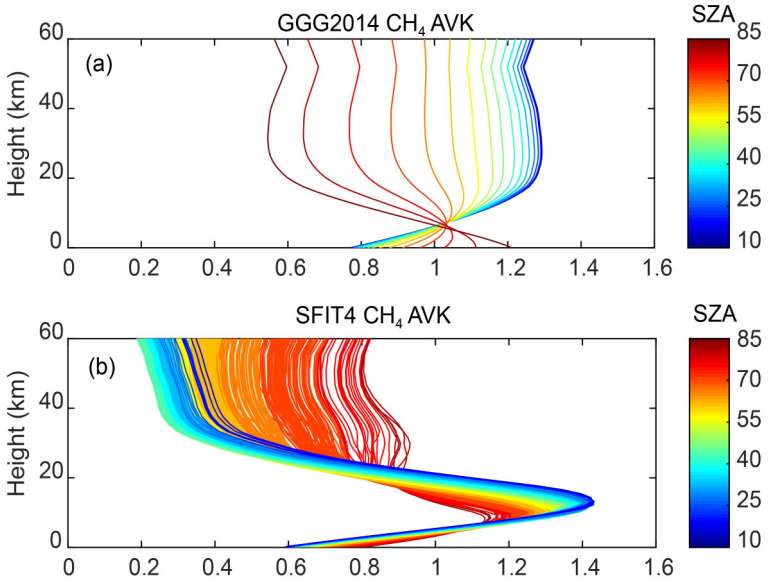

Fig. 3. Column averaging kernel (AVK) of the CH_4 retrieval in the (a) GGG2014 and (b) SFIT4 codes, colored with different solar zenith angels (SZAs).

inversion is sensitive to the whole atmosphere. However, in reality, the sensitivity to the atmospheric state of the AVK varies by height. For example, for TCCON, the total amount of CH_4 is always sensitive to the troposphere (> 0.8), regardless of SZA. However, in the stratosphere, the total amount of CH_4 varies from 1.2 to 0.6 as the SZA varies from 10° to 85°.

This is mainly because, as the Sun obliquely enters the atmosphere (as SZA increases), pressure broadening in the stratosphere contributes to a narrower linewidth than the saturated central region for gases with saturated absorption lines. Therefore, as the mass of air increases, the line becomes more saturated, so the AVK of the stratosphere is partially reduced, resulting in the total amount of column inversions becoming insensitive to stratospheric information. For the AVK in NDACC, the inversion CH_4 column mole fraction is more sensitive to the troposphere and the lower stratosphere.

In addition to the total column, SFIT4 can retrieve the partial column of CH_4. The profiling capability is not only important for CH_4 source or sink research applications, but is also advantageous when validating column-averaged CH_4 obtained from satellites (Sepúlveda et al., 2014). The degree of freedom (DOF) of the NDACC-retrieved profile (from ground to the top of the atmosphere) of CH_4 is 2.23±0.18 (1δ), meaning that there are two independent pieces of information in the vertical distribution of CH_4. According to the DOF, we divide the vertical distribution of CH_4 into two independent parts: one from the ground to 12.2 km (representing the troposphere), and the second from 12.2 to 60 km (representing the stratosphere). The DOF in each part is approximately 1, which means that the signal information in each part is independent (Fig. 4). We calculated the dry-air column-averaged mole fractions of CH_4 in the troposphere ($X_{CH_4,tr}$) and stratosphere ($X_{CH_4,st}$) (Zhou et al., 2018), as follows:

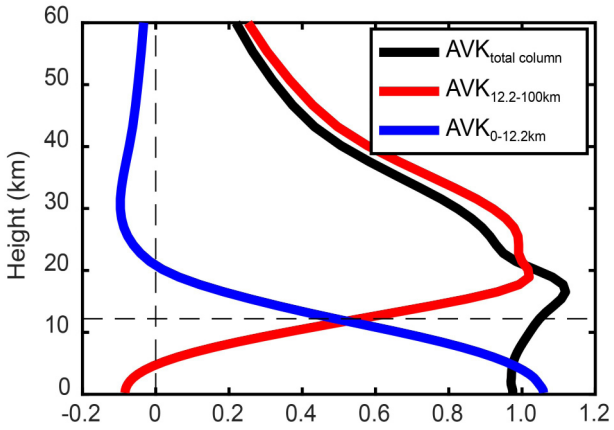

Fig. 4. Total column averaging kernel (black), together with the partial column averaging kernels of two individual layers (CH_4: surface–12.2 km, partial column DOFs=1, and 12.2–60 km, partial column DOFs=1) of one typical NDACC retrieval in Xianghe.

$$X_{CH_4,tr} = PC_{CH_4,tr}/PC_{air\_dry,tr} = PC_{CH_4,tr}/(PC_{air\_wet,tr} - PC_{H_2O,tr}), \quad (7)$$

$$X_{CH_4,st} = PC_{CH_4,st}/PC_{air\_dry,st}, \quad (8)$$

where $PC_{CH_4,tr}$, $PC_{H_2O,tr}$, $PC_{air\_dry,tr}$, and $PC_{air\_wet,tr}$ are the partial columns of CH_4, H_2O, dry air, and wet air in the troposphere, and $PC_{CH_4,st}$ and $PC_{air\_dry,st}$ are the partial columns of CH_4 and dry air in the stratosphere, respectively.

Combined in-situ and FTIR measurements provided information about CH_4 in three vertical layers: near the ground, in the troposphere, in the stratosphere, and in the total atmospheric column. This enabled us to analyze the temporal and vertical distribution of CH_4 in source emission areas.

3.2.3. *Uncertainty budget*

TCCON is a well-developed worldwide observation network. Details of the sources of known uncertainty are described in Wunch et al. (2011). For X_{CH_4}, the largest sources of error are observer-sun Doppler stretch, shear misalignment, continuum curvature, a priori profiles, and angular misalignment. The total X_{CH_4} error, i.e., the sum of each individual uncertainty, is below 0.5% until the SZA is above ~85°. Yang et al. (2019) proved that the FTIR at the Xianghe site meets the TCCON requirements, and the instrument is in good working condition. Thus, it is reasonable to believe that the X_{CH_4} uncertainty budget of this site when using the TCCON observation mode is consistent with other TCCON sites.

For the NDACC observation mode, according to Rodgers (2000), the difference between the true and retrieved state of the atmosphere can be written as follows:

$$\boldsymbol{x}_r - \boldsymbol{x} = (\boldsymbol{A} - \boldsymbol{I})(\boldsymbol{x} - \boldsymbol{x}_a) + \boldsymbol{G}\boldsymbol{K}_b\boldsymbol{\varepsilon}_b + \boldsymbol{G}\boldsymbol{\varepsilon}_y\,, \tag{9}$$

where $\boldsymbol{I}$ is the identity matrix, $\boldsymbol{\varepsilon}_b$ is the error in forward model parameters, and $\boldsymbol{\varepsilon}_y$ is the measurement error. According to Eq. (9), the total error is divided into three error sources: smoothing error, forward model parameter error, and measurement error (Senten et al. 2008). Table 2 shows the values of those errors for a regular observation. In summary, the systematic and random errors of the NDACC total column are about 3.3% and 1.7%, respectively.

3.3. *The CarbonTracker-CH_4 system*

CarbonTracker-CH_4 is an assimilation system for atmospheric CH_4 developed by the National Oceanic and Atmospheric Administration (NOAA). Using observations from surface stations and towers, CarbonTracker-CH_4 assimilates global atmospheric CH_4 into TM5 (Transport Model 5; Liu et al., 2016). We used the current release, CT2010, to analyze the atmospheric CH_4 mole fractions in Xianghe at the surface. In CarbonTracker-CH_4, CH_4 emissions into the atmosphere are estimated separately for natural and anthropogenic sources. Natural sources include oceans, wetlands, soil, and insects and wild animals. The anthropogenic sources include emissions from fires, coal, oil and gas production, animals, rice cultivation and waste. We used daily averages from 2010 to determine the contributions from different anthropogenic sources in Xianghe.

4. Results and discussion

4.1. *Comparison between in-situ and FTIR total column measurements*

Figure 5 shows the seasonal variation of CH_4 measured by the Picarro G2301 (mole fraction near the ground) and FTIR (total column-averaged dry-air mole fraction of CH_4). The means (standard deviation) of the CH_4 mole fraction measurements are as follows: 2.2049 ppm (0.0945 ppm) for the Picarro, 1.8839 ppm (0.0129 ppm) for TCCON, and 1.9234 ppm (0.0193 ppm) for NDACC. It is clear that the mole fraction of CH_4 near the ground is much higher than the total column-averaged CH_4. All three sets of measurements had high values in summer, later autumn, and early winter. A minimum in CH_4 in March and April was observed by both in-situ and FTIR measurements. The total columns of CH_4 based on the TCCON and NDACC measurements are similar, and the average X_{CH_4} for NDACC is about 39.5 ppb higher than TCCON. The correlation coefficient between the daily means derived from the Picarro and FTIR measurements is 0.21, indicating that the daily variation of CH_4 near the ground is different from that in the total column. The near-surface CH_4 is strongly impacted by the local emissions and sinks, while the FTIR total column amounts combine the contributions from the boundary layer, free troposphere, stratosphere, and above.

Zhang and Qun (2011) analyzed the total column amount of CH_4 in China using SCIAMACHY(Scanning Imaging Absorption Spectrometer for Atmospheric Chartography) satellite observations. They found that concentrations of CH_4 are higher in summer and lower in winter, which was attributed to biological sources in association with soil temperature and land moisture. The warm and wet soil conditions, leading to higher production in summer, provide a suitable environment for microbes to produce CH_4 by anaerobic respiration (Freeman et al., 2002, Hao et al., 2005, He et al., 2019). This is one possible reason for the total column amount of CH_4 seen in Xianghe during summer. However, the total column of CH_4 in Xianghe in winter was higher than that in spring. These findings indicate that the seasonal variation in total column amounts of CH_4 in Xianghe is not fully attributable to biological sources.

4.2. *Seasonal cycle of CH_4 in the troposphere and stratosphere*

CH_4 varies with altitude, as shown in Fig. 6. In the troposphere, the average CH_4 concentration was 2.0599 ± 0.0224 ppm, with two maxima in August and December (2.0977 ± 0.0259 and 2.0608 ± 0.0228 ppm, respectively), and two minima in October and March (2.0387 ± 0.0177 and 2.0196 ± 0.0134 ppm, respectively). Compared with the in-situ measurements at the surface, CH_4 is much more well-mixed in the troposphere than near the surface. The variation in the tropospheric column of CH_4 is close to that in the in-situ measurements near the ground.In the stratosphere, the annual average CH_4 concentration was 1.6498 ± 0.0496 ppm, and was

Table 2. CH_4 uncertainty budget in NDACC observation mode.

Smoothing error	Measurement error	Forward model parameter error			Total random error
		Interference species error	Temperature (systematic)	Line intensity error (CH_4)	
0.117[%]	0.104[%]	0.014[%]	1.426[%]	2.938[%]	1.737[%]

higher in the summer (1.7374 ± 0.0267 ppm) and lower in the winter (1.5700 ± 0.0625 ppm).

Several studies show that the distribution of atmospheric trace gases is related to the Brewer–Dobson circulation (BDC); in midlatitudes, the stratosphere–troposphere exchange (STE) caused by tropopause folding can influence the vertical distribution of long-lived gases, such as CH_4, N_2O, and O_3 (Yang and Lü, 2004; Simmonds et al., 2013; Fan et al., 2014). Simmonds et al. (2013) reported that the BDC is driven by vertically propagating Rossby and gravity waves. When these waves break in the stratosphere, the speed of westerly airflow decreases, which results in high-latitude convergence and the descent of stratospheric air into the troposphere (Lu and Ding, 2013). For detailed characterization of BDC, residual circulation is often used to analyze air mass transport. Many studies have proven that such STE in midlatitudes is dominated by transportation from the stratosphere to the troposphere, which is strong in winter and spring, and weak in summer and autumn (Yang et al., 2003; Simmonds et al., 2013; Fan et al., 2014). Fan et al. (2014) showed that the center of the upwelling residual circulation at 150 hPa tends to shift northwards between April and August, and southwards between September and February of the following year. More specifically, this upwelling center can be situated at 40°N in the summer, which is very close to the study region of Xianghe. Therefore, the CH_4 measurements in Xianghe could provide information about CH_4 transport between the stratosphere and troposphere.

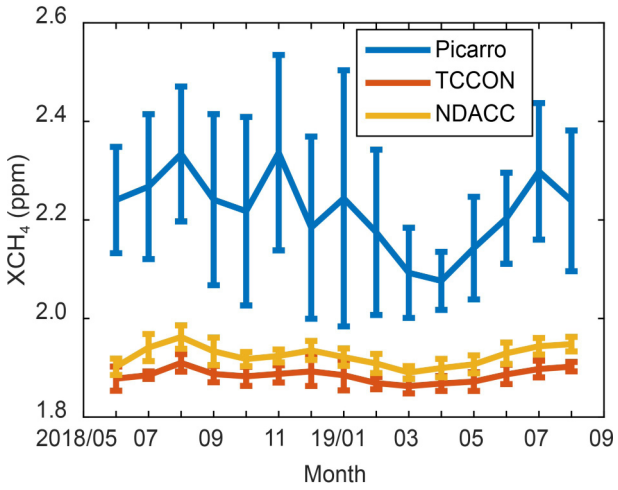

Fig. 5. Seasonal variation of CH_4 measured by Picarro and FTIR. The error bar is 1$\sigma$for all the observed data within that month.

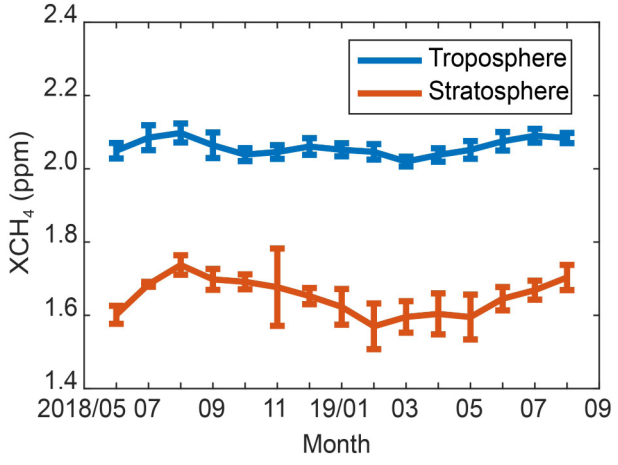

Fig. 6. Seasonal variations in two different layers: the free troposphere (blue line) and stratosphere (red line). The error bar is 1σ for all the observed data within that month.

Figure 7 shows the annual-averaged X_{CH_4} profile in Xianghe, as well as the difference between the summer- and annual-averaged, and winter- and annual-averaged, X_{CH_4} values. There is a positive X_{CH_4} value of 0.04 ppm in summer, and a negative value of −0.05 ppm in winter. We deduce that the higher value of CH_4 in the stratosphere from June to August is related to upward vertical motion during that period, due to air from the troposphere entering the stratosphere and increasing the CH_4 mole fraction. Conversely, the lower value of stratospheric CH_4 in winter could be due to downward vertical motion.

In summary, we found that CH_4 in the troposphere was relatively well-mixed, with little variation. There were two peaks: one in the summer, caused by local sources of CH_4, and one in winter, resulting from fewer hydroxyl radicals.

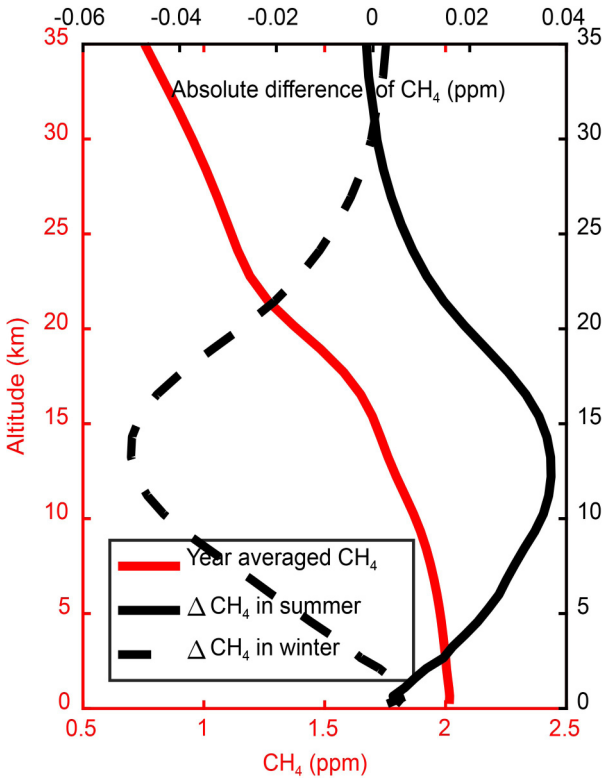

Fig. 7. The yearly averaged profile of CH_4 in Xianghe (red line), and the profile of the difference between the mean CH_4 profile in summer with the yearly averaged one (black solid line), and the profile of the difference between the mean CH_4 profile in winter with the yearly averaged one (black dashed line).

In the stratosphere, the mixing ratio of CH_4 could be influenced by the STE, which reaches a maximum in summer and a minimum in winter.

4.3. *Diurnal variation of CH_4 near the ground*

We mainly attribute the diurnal changes in the CH_4 mole fraction to three factors: local source emissions, diurnal variation of the boundary layer (which could impact the dilution of CH_4), and the rate of oxidation by OH free-radicals (Fang et al., 2012). At most background stations, the CH_4 mole fraction is lower during the daytime than at night, since transport and photochemical sinks are more influential during the day (Fang et al., 2012). However, in some source areas, such as rice paddies, CH_4 emission flux increases with temperature during the daytime, reaching a maximum value at 1500LT. Thereafter, the CH_4 flux decreases with temperature (Lu et al., 2015).

It is obvious that, in source areas, the diurnal variation of CH_4 is mostly influenced by local emissions. Xianghe is a typical source area; diurnal variation of CH_4 from in-situ measurements at this site are shown in Fig. 8. In spring, summer, and autumn, the CH_4 mole fraction was higher at night (1800–0600 LT) than during the daytime (0600–1800 LT); it grows slowly but continuously, peaking at 2300 LT, before decreasing rapidly until 0600 LT the next day. However, in winter, there was no apparent difference in the CH_4 mole fraction between daytime and nighttime; it increased between 0600 and 1500 LT and was stable between 1500 and 2400 LT, after which it decreased as in all other seasons.

Recall that there are three factors that may affect the diurnal variation of CH_4 at the surface. First, OH free-radical oxidation is a relatively slow process during the day, having a rate of 360×10^{12}–530×10^{12} gyr^{-1} (about 0.179 ppm yr^{-1}); this cannot explain the observed dramatic change in CH_4 (Wang, 1991). Aside from during the winter, the inflexion points of the CH_4 signal occurred in the morning (~0600 LT) and afternoon (~1600–1700 LT). Assuming strong CH_4 emissions at the surface, concentrations are diluted in the deeper daytime boundary layer, whereas at nighttime CH_4 accumulates in the shallower boundary layer. This results in the CH_4 mole fraction during the daytime being lower than

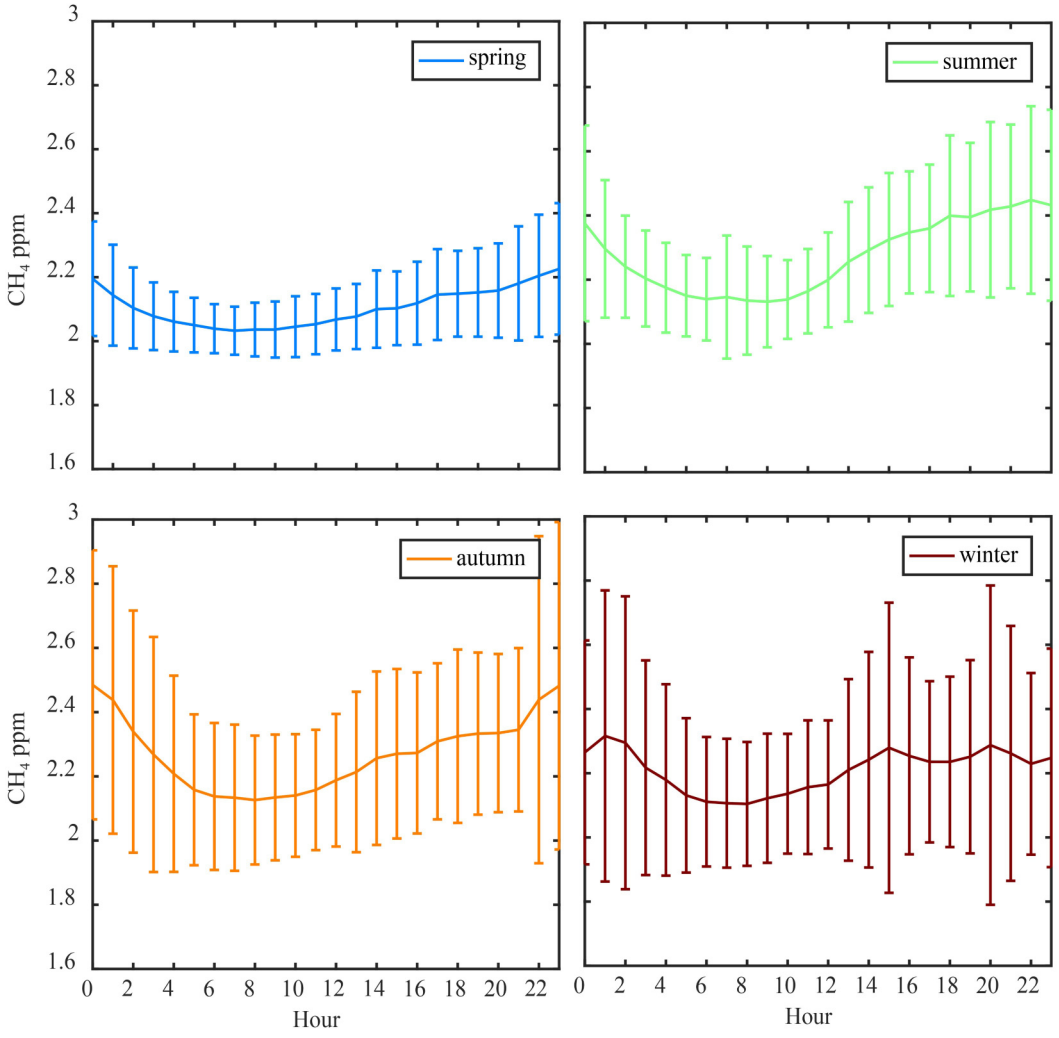

Fig. 8. Diurnal variation of CH_4 at the surface from spring to winter. The time units are in local time (+8 h UTC). The error bar is 1σ for all the observed hourly mean data within that season at that local time.

at night, thus showing the influence of the boundary layer on the diurnal variations of CH_4.

Some studies show that the diurnal variation of emissions from landfill waste is greater at night than during the daytime (Börjesson and Svensson, 1997; Chen et al., 2008). In winter, the inflexion point was in the afternoon (~1500 LT), which is relatively different than for the other seasons. This difference may be a result of strong anthropogenic emissions at the surface close to Xianghe.

The Beijing–Tianjin–Hebei region is dominated by domestic landfill waste and wastewater treatment (Le et al., 2012; Huang et al., 2019). Huang et al. (2019) found that CH_4 emissions from domestic landfill waste and wastewater treatment accounts for more than 30% of total CH_4 emissions in Beijing and Tianjin. However, the proportion of arable land in the Beijing–Tianjin–Hebei region gradually decreased between 1990 and 2015, by about 50% (Gong et al., 2019). Therefore, CH_4 emission sources may have changed as arable land availability decreased, and as wastewater and domestic garbage treatment increased. Also, in 2018, a new domestic waste site was created about 8 km away from the Xianghe site. We deduce that CH_4 emissions in Xianghe are most likely related to domestic landfill waste and wastewater treatment. Further investigation is needed to understand the diurnal variation of emissions, which in turn could help us to better understand the diurnal variation of CH_4 in particular.

4.4. *CarbonTracker-CH_4 model simulations*

We used CarbonTracker model simulations to analyze emission contributions from different sources in Xianghe. Figure 9a shows the seasonal variation of the CH_4 mole fraction in 2010 from six different sources: fossil fuels; insects/wild animals; rice cultivation and waste; wetlands and soil; oceans; and wildfires. Fossil fuels, wildfires, and oceans are not as important as the other sources, only accounting for about 15% of total emissions in Xianghe. The most important sources are animals, rice cultivation, and waste, which accounted for about 32.6% of the total emissions.

The largest seasonal variation in emissions was found for wetlands, soil, oceans, and insects/wild animals; emissions were higher in the summer (~700 ppb in August) and lower in other seasons (~420 ppb). This helps explain the relatively high values measured in-situ, especially in August. A small peak in December for agriculture waste was simulated, which may explain the measured peak of the CH_4 mole fraction near the surface at this time.

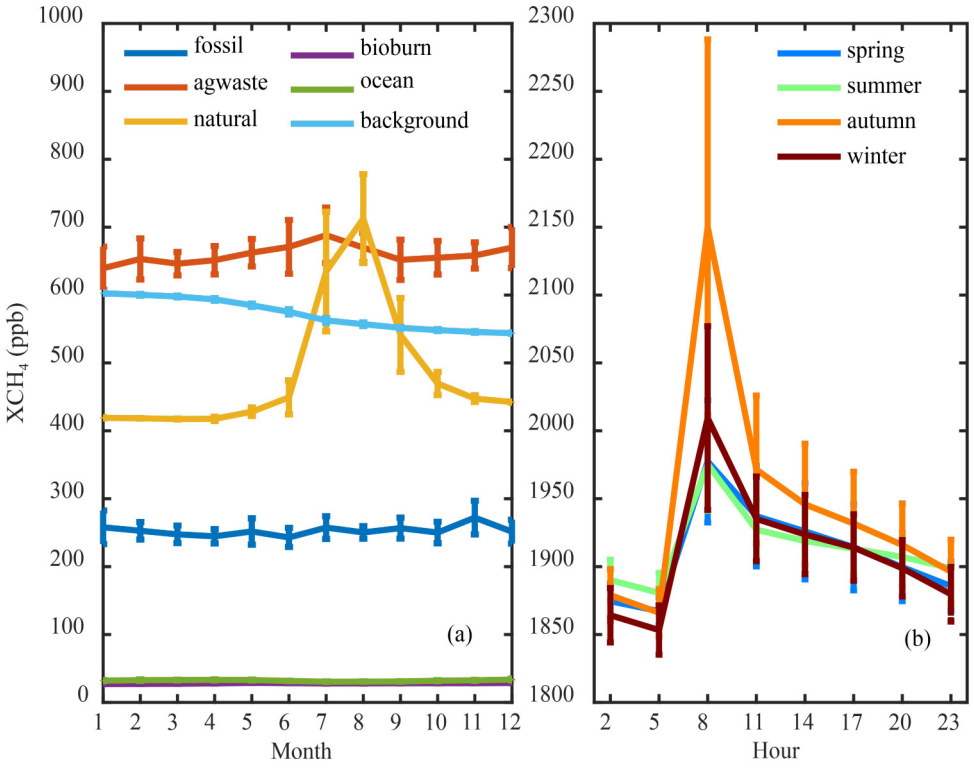

Fig. 9. Model results of (a) seasonal variation of the mean and standard deviation of CH_4 mole fraction near the surface due to different sources, wherein the dark blue line represents emissions from fossil fuels, the red line represents emissions from animals, rice cultivation and waste, the yellow line represents natural emissions from wetlands, soil, oceans and insects/wild animals, the purple line represents emissions from the oceans, and the light blue line represents emissions from fires. The error bar is 1σ for all the simulated daily mean data within that season; and (b) daily variation of the CH_4 near the surface from spring to winter. The time units are local time (+8 h UTC). The error bar is 1σ for all the simulated hourly mean data within that season at that local time.

According to the modeled diurnal variation of the CH_4 mole fraction (Fig. 9b), maximum values occurred every day at 0800 LT from spring to winter; this was not shown by the in-situ measurements. Since the model simulation was for 2010 (about nine years ago at the time of writing), sources of CH_4 may have changed greatly, especially with regard to domestic landfill waste and wastewater treatment, which has recently played a more important role.

5. Conclusions

Atmospheric CH_4 mole fractions were measured by in-situ and FTIR instruments in Xianghe beginning in June 2018. In-situ observations provided information near the ground, and FTIR measurements provided information on total column values of CH_4, as well as partial columns in the troposphere and stratosphere, based on TCCON and NDACC measurements.

The mean (standard deviation) of the CH_4 mole fraction near the ground measured by the Picarro instrument was 2.2049 ppm (0.0945 ppm). The mean (standard deviation) X_{CH_4} measured by FTIR was 1.8839 ppm (0.0129 ppm) based on TCCON data and 1.9234 ppm (0.0193 ppm) based on NDACC data. The CH_4 mole fraction near the ground was about 13% larger than for X_{CH_4}, since there are strong CH_4 emissions at the surface near Xianghe. The CH_4 mole fraction in the stratosphere was much lower than that in the troposphere. Similar seasonal variations of CH_4 were found near the ground, in the troposphere, and in the stratosphere. The CH_4 mole fraction in the stratosphere appeared to change with season, which could be due to the influence of STE.

The CH_4 mole fraction near the ground reached its maximum value near midnight (~2200–2300 LT), with its minimum value occurring at 0600–0700 LT. The daily maximum values in summer were relatively higher than in other seasons, at nearly 2.4 ppm.

Comparing CarbonTracker-CH_4 model simulations with our observations near the ground in Xianghe, we found that the model can reproduce the peak value of the CH_4 mole fraction in summer, but underestimates the peak value in winter. The modeled and measured daily variation of the CH_4 mole fraction differed.

In summary, we analyzed the temporal and vertical distributions of CH_4 in source emission areas using Picarro and FTIR measurements. The vertical distributions could be very useful for understanding the source emissions at such a polluted site.

Acknowledgements. This research was funded by the National Key R&D Program of China (Grant Nos. 2017YFB 0504000 and 2017YFC150 1701) and the National Natural Science Foundation of China (Grant No. 41975035). We want to thank the TCCON community for sharing the GGG2014 retrieval code, the NDACC community for sharing the SFIT4 retrieval code, and NOAA for providing the CarbonTracker-CH_4 Data Assimilation Product. We also want to thank Weidong NAN, Qing YAO, and Qun CHEN (Xianghe site) for the maintenance of the in-situ and FTIR measurements at Xianghe.

REFERENCES

Börjesson, G., and B. H. Svensson, 1997: Seasonal and diurnal methane emissions from a landfill and their regulation by methane oxidation. *Waste Management & Research*, **15**, 33–54, https://doi.org/10.1006/wmre.1996.0063.

Chen, I.-C., U. H. Hegde, C. H. Chang, and S. S. Yang, 2008: Methane and carbon dioxide emissions from closed landfill in Taiwan. *Chemosphere*, **70**, 1484–1491, https://doi.org/10.1016/j.chemosphere.2007.08.024.

Crippa, M., and Coauthors, 2018: Gridded emissions of air pollutants for the period 1970–2012 within EDGAR v4.3.2. *Earth System Science Data*, **10**, 1987–2013, https://doi.org/10.5194/essd-10-1987-2018.

De Mazière, M., and Coauthors, 2018: The Network for the Detection of Atmospheric Composition Change (NDACC): History, status and perspectives. *Atmospheric Chemistry and Physics*, **18**, 4935–4964, https://doi.org/10.5194/acp-18-4935-2018.

Duncan, W. T., and T. N. Truong, 1995: Thermal and vibrational - state selected rates of the CH_4+ Cl↔ HCl+ CH_3 reaction. *The Journal of Chemical Physics*, **103**, 9642–9652, https://doi.org/10.1063/1.470731.

Esler, M. B., D. W. T. Griffith, S. R. Wilson, and L. P. Steele, 2000: Precision trace gas analysis by FT-IR spectroscopy. 1. Simultaneous analysis of CO_2, CH_4, N_2O, and CO in air. *Analytical Chemistry*, **72**, 206–215, https://doi.org/10.1021/ac9905625.

Fan, W. X., H. Y. Wang, W. G. Wang, F. Y. Yang, and W. C. Zhang, 2014: Temporal-spatial structural switch and evolution characteristics of the residual circulation in the different seasons. *Acta Meteorologica Sinica*, **72**, 542–553, https://doi.org/10.11676/qxxb2014.043. (in Chinese with English abstract)

Fang, S. X., Z. Li, L. X. Zhou, and L. Xu, 2012: Variation of CH_4 concentrations at Yunnan Xianggelila background station in China. *Acta Scientiae Circumstantiae*, **32**, 2568–2574, https://doi.org/10.13671/j.hjkxxb.2012.10.033.

Freeman, C., G. B. Nevison, H. Kang, S. Hughes, B. Reynolds, and J. A. Hudson, 2002: Contrasted effects of simulated drought on the production and oxidation of methane in a mid-Wales wetland. *Soil Biology and Biochemistry*, **34**, 61–67, https://doi.org/10.1016/S0038-0717(01)00154-7.

Fung, I., J. John, J. Lerner, E. Matthews, M. Prather, L. P. Steele, and P. J. Fraser, 1991: Three - dimensional model synthesis of the global methane cycle. *J. Geophys. Res.*, **96**, 13 033–13 065, https://doi.org/10.1029/91JD01247.

Gong, Y. L., J. T. Li, and Y. X. Li, 2019: Spatiotemporal characteristics and driving mechanisms of arable land in the Beijing-Tianjin-Hebei region during 1990-2015. *Socio-Economic Planning Sciences*, https://doi.org/10.1016/j.seps.2019.06.005.

Hao, Q. J., Y. S. Wang, C. S. Jiang, C. K. Wang, and M. X. Wang, 2005: A review on methane emission from wetlands. *Chinese Journal of Ecology*, **24**, 170–175, https://doi.org/10.13292/j.1000-4890.2005.0230.

Hase, F., J. W. Hannigan, M. T. Coffey, A. Goldman, M. Höpfner, N. B. Jones, C. P. Rinsland, and S. W. Wood, 2004: Intercomparison of retrieval codes used for the analysis of high-resolution, ground-based FTIR measurements. *Journal of Quantitative Spectroscopy and Radiative Transfer*, **87**, 25–52, https://doi.org/10.1016/j.jqsrt.2003.12.008.

He, F. J., H. B. Han, X. Q. Ma, J. S. Zhang, and S. J. Sun, 2019: Characteristics and influence factors of CH_4 flux in different areas of Longbaotan marsh wetland. *Ecology and Environmental Sciences*, **28**, 803–811, https://doi.org/10.16258/j.cnki.1674-5906.2019.04.020. (in Chinese with English abstract)

Heilig, G. K., 1994: The greenhouse gas methane (CH_4): Sources and sinks, the impact of population growth, possible interventions. *Population and Environment*, **16**, 109–137, https://doi.org/10.1007/BF02208779.

Huang, M. T., T. J. Wang, X. F. Zhao, X. D. Xie, and D. Y. Wang, 2019: Estimation of atmospheric methane emissions and its spatial distribution in China during 2015. *Acta Scientiae Circumstantiae*, **39**, 1371–1380, https://doi.org/10.13671/j.hjkxxb.2018.0463. (in Chinese with English abstract)

IPCC, 2014: Climate Change 2013: *The Physical Science Basis: Working Group I Contribution to the Fifth Assessment Report of the Intergovernmental Panel on Climate Change*. Cambridge University Press.

Janssens-Maenhout, G., and Coauthors, 2019: EDGAR v4.3.2 global atlas of the three major greenhouse gas emissions for the period 1970–2012. *Earth System Science Data*, **11**, 959–1002, https://doi.org/10.5194/essd-11-959-2019.

Kaplan, J. O., G. Folberth, and D. A. Hauglustaine, 2006: Role of methane and biogenic volatile organic compound sources in late glacial and Holocene fluctuations of atmospheric methane concentrations. *Global Biogeochemical Cycles*, **20**, GB2016, https://doi.org/10.1029/2005GB002590.

Kirschke, S., and Coauthors, 2013: Three decades of global methane sources and sinks. *Nature Geoscience*, **6**, 813–823, https://doi.org/10.1038/ngeo1955.

Laurent, O., 2015: ICOS Atmospheric Station Specifications, ICOS. [Available online from https://icos-atc.lsce.ipsl.fr/?q=filebrowser/download/8681.]

Le, Q., G. J. Zhang, and Z. Wang, 2012: Preliminary estimation of methane emission and its distribution in China. *Geographical Research*, **31**, 1559–1570. (in Chinese with English abstract)

Liu, M., L. P. Lei, D. Liu, and Z.-C. Zeng, 2016: Geostatistical analysis of CH_4 columns over Monsoon Asia using five years of GOSAT observations. *Remote Sensing*, **8**, 361, https://doi.org/10.3390/rs8050361.

Lu, C. H., and Y. H. Ding, 2013: Progress in the Study of Stratosphere-Troposphere Interaction. *Advances in Meteorological Science and Technology*, **3**, 6–21, https://doi.org/10.3969/j.issn.2095-1973.2013.02.001. (in Chinese with English abstract)

Lu, Y., Zhang, W., L i, T. T., and Y. J., Zhou, 2015: Progress in the simulation of the impacts of sources and sinks on the tempo-spatial variations of the atmospheric. *Advances in Earth Science*, **30**(7), 763–772, https://doi.org/10.11867/j.issn.1001-8166.2015.07.0763. (in Chinese with English abstract)

Mann, M. E., 2014: Earth will cross the climate danger threshold by 2036. *Sci. Amer.*, **4**, 78–81, https://doi.org/10.1038/scientificamerican0414-78.

Notholt, J., R. Neuber, O. Schrems, and T. V. Clarmann, 1993: Stratospheric trace gas concentrations in the Arctic polar night derived by FTIR-spectroscopy with the Moon as IR light source. *Geophys. Res. Lett.*, **20**, 2059–2062, https://doi.org/10.1029/93GL01971.

Rodgers, C. D., 2000: *Inverse Methods for Atmospheric Sounding: Theory and Practice*. World Scientific, https://doi.org/10.1142/9789812813718.

Senten, C., and Coauthors, 2008: Technical Note: New ground-based FTIR measurements at Ile de La Réunion: Observations, error analysis, and comparisons with independent data. *Atmospheric Chemistry and Physics.*, **8**, 3483–3508, https://doi.org/10.5194/acp-8-3483-2008.

Sepúlveda, E., and Coauthors, 2014: Tropospheric CH_4 signals as observed by NDACC FTIR at globally distributed sites and comparison to GAW surface in situ measurements. *Atmospheric Chemistry and Physics*, **7**, 2337–2360, https://doi.org/10.5194/amt-7-2337-2014.

Simmonds, P. G., and Coauthors, 2013: Interannual fluctuations in the seasonal cycle of nitrous oxide and chlorofluorocarbons due to the Brewer - Dobson circulation. *J.Geophys. Res.*, **118**, 10 694–10 706, https://doi.org/10.1002/jgrd.50832.

Toon, G. C., and D. Wunch, 2015: A stand-alone a priori profile generation tool for GGG2014 release (Version GGG2014.R0), CaltechDATA, https://doi.org/10.14291/tccon.ggg2014.priors.r0/1221661.

Toon, G. C., C. B. Farmer, P. W. Schaper, L. L. Lowes, and R. H. Norton, 1992: Composition measurements of the 1989 Arctic winter stratosphere by airborne infrared solar absorption spectroscopy. *J.Geophys. Res.*, **97**, 7939–7961, https://doi.org/10.1029/91JD03114.

Wang, M. X., 1991: *Atmospheric Chemistry*. China Meteorological Press, 122–123. (in Chinese)

Wunch, D., and Coauthors, 2011: The total carbon column observing network. *Philosophical Transactions of the Royal Society A: Mathematical. Proceedings of the Royal Society A: Mathematical, Physical and Engineering Sciences*, **369**, 2087–2112, https://doi.org/10.1098/rsta.2010.0240.

Yang, J., and D. R. Lü, 2003: Progress in the study of stratosphere-troposphere exchange. *Advance in Earth Sciences*, **3**, 53–58. (in Chinese with English abstract)

Yang, J., and D. R. Lü, 2004: Diagnosed seasonal variation of stratosphere-troposphere exchange in the northern hemisphere by 2000 Data. *Chinese Journal of Atmospheric Sciences*, **28**, 294–300, https://doi.org/10.3878/j.issn.1006-9895.2004.02.12. (in Chinese with English abstract)

Yang, Y., and Coauthors, 2019: A new site: Ground-based FTIR XCO2, XCH_4 and XCO measurements at Xianghe, China. *Earth System Science Data*, https://doi.org/10.5194/essd-2019-172.

Zhang, D. Y., and H. Liao, 2015: Advances in the research on sources and sinks of CH_4 and observations and simulations of CH_4 concentrations. *Advances in Meteorological Science and Technology*, **5**, 40–47, https://doi.org/10.3969/j.issn.2095-1973.2015.01.005. (in Chinese with English abstract)

Zhang, G. J., and L. Qun, 2011: Distribution of CH_4 Column in China using SCIAMACHY data. *Geospatial Information*, **9**, 115–117, https://doi.org/10.3969/j.issn.1672-4623.2011.04.041. (in Chinese with English abstract)

Zhou, M. Q., and Coauthors, 2018: Atmospheric CO and CH_4 time series and seasonal variations on Reunion Island from ground-based in situ and FTIR (NDACC and TCCON) measurements. *Atmospheric Chemistry and Physics*, **18**, 13 881–13 901, https://doi.org/10.5194/acp-18-13881-2018.

Zhou, M. Q., and Coauthors, 2019: An intercomparison of total column-averaged nitrous oxide between ground-based FTIR TCCON and NDACC measurements at seven sites and comparisons with the GEOS-Chem model. *Atmospheric Measurement Techniques*, **12**, 1393–1408, https://doi.org/10.5194/amt-12-1393-2019.